

This is a non-peer-reviewed preprint submitted to EarthArXiv.

This manuscript has been submitted for publication in *Bulletin* of the American Meteorological Society (BAMS). Copyright in this manuscript may be transferred without further notice. Please note the manuscript has yet to be formally accepted for publication. Subsequent versions of this manuscript may have slightly different content. If accepted, the final version of this manuscript will be available via the 'Peer-reviewed Publication DOI' link on the right-hand side of this webpage. Please feel free to contact any of the authors; we welcome feedback.

17	Biases due to widespread use of low-cost sensors for urban heat stress
18	assessments
19	Sarah Berk, <sup>a</sup> , TC Chakraborty <sup>b</sup> , Angel Hsu <sup>a</sup>
20	<sup>a</sup> University of North Carolina at Chapel Hill, Chapel Hill, NC
21	<sup>b</sup> Pacific Northwest National Laboratory, Richland, WA
22	
23	Corresponding authors: TC Chakraborty, tc.chakraborty@pnnl.gov, Angel Hsu,
24	angel.hsu@unc.edu
25	

26 ABSTRACT

27

28

29

30

31

32

33

34

35

36

37

38

39

40

41

42

43

44

45

46

47

48

49

50

51

52

53

54

55

56

Urban heat stress is an area of critical research interest due to its relevance for public health and policy. Given the lack of operational-grade weather stations within cities, different types of low-cost sensors have been used to assess urban heat stress. However, these sensors are traditionally not designed for capturing fine scale differences in temperature and humidity (i.e., the main components of moist heat), which are expected across a city, and their siting is often suboptimal due to logistical challenges. Here, through several calibration exercises over lawn and rooftop settings using 41 Kestrel sensors, we demonstrate significant issues with the use of such low-cost sensors for urban heat stress assessments. Issues stem from use of sensors without radiation shields, and even with cheaper non-aspirated shields, exposure to confounding environmental factors, and local land cover influences. Unshielded sensors overestimated temperature by up to 0.7 °C relative to shielded counterparts. Within unaspirated radiation shields, daytime measurement error was strongly correlated with diurnal temperature range (lawn r = 0.85; unshaded rooftop r = 0.98). Humidity cross-sensor variability exhibited a weaker correlation with its diurnal range. Heat index, derived from temperature and humidity, combined biases in the two measurements, magnifying resulting errors (4.7% increase compared to standard error for temperature). Finally, sensors near anthropogenic heat sources showed cross-sensor variability up to seven times higher than interference free sites. Based on these potential mismeasurements in urban heat stress gradients seen using inexpensive sensors, we provide recommendations on their appropriate deployment in urban environments.

#### SIGNIFICANCE STATEMENT

Heat stress is a particular concern in cities, where temperatures are often higher than in nearby rural areas. To identify which neighborhoods face the greatest risks, communities and researchers have increasingly turned to low-cost sensors to measure temperature and humidity. Our study shows that these low-cost sensors must be used with caution when comparing conditions across a city, especially in hot and humid conditions. Inaccurate readings risk muting or magnifying the true extent of heat exposure and misguiding resilience planning. We highlight the importance of proper shielding and placement of sensors, and underscore the need for stricter standards to ensure reliable location-based comparisons of temperature and humidity.

Low-cost sensors are widely used to monitor urban heat, but shielding, siting, and accounting for local interferences are critical for robust intra-city comparisons.

## 1. Introduction

With global climate change and rapid urbanization, the need to address extreme heat is particularly critical in cities, which frequently experience elevated air temperatures (AT) in relation to their rural references or the urban heat island (UHI) effect (Mohajerani et al., 2017). Similarly, urbanization reduces relative humidity (RH), the urban dry island (UDI) effect, together modulating moist heat, a function of both temperature and humidity, within cities (Chakraborty et al., 2022). Across many regions of the United States, humidity can amplify heat stress burden over what temperature alone would suggest (Narayanan et al., 2025), as high humidity limits evaporative cooling through sweat (McGregor & Vanos, 2018). 

Combined with the high population densities of urban centers, the increased health risks associated with moist heat can have disproportionately higher impacts in cities. The magnitude of heat hazard is not uniform across a city, and varies significantly due to local differences in land cover, building morphology, and surface materials. Accurately estimating intra-urban patterns of AT and RH is therefore essential for comparing physiologically relevant heat hazard across different parts of a city (Chakraborty et al., 2023; Hsu et al., 2021). Furthermore, assessing spatial unevenness in heat exposure at policy-relevant scales is needed for guiding targeted mitigation strategies (Chakraborty et al., 2022) and informing climate resilience (Martilli et al., 2020).

The drivers of urban climate operate on relatively small spatial scales, making conventional meteorological datasets, such as reanalysis products (e.g., ERA5 (Hersbach et al., 2020)) too coarse to capture these variations (Y. Li et al., 2024; Nogueira et al., 2022). Satellite-sensed land surface temperature provides higher resolution (100m to 1 km) but is less relevant for human health and comfort than AT and moist heat stress indices (Chakraborty et al., 2022; Venter et al., 2021).

While AT and RH are common meteorological variables, standard weather stations are rarely located within the urban environment (J. Li et al., 2023; Muller et al., 2013); thus unable to accurately capture intra-urban variabilities of thermal comfort and health risk.

"Urban" weather stations are often located at nearby airports, thus only representing conditions at a single point, often away from the core urban fabric (J. Li et al., 2023). These stations are also required to follow strict siting guidelines from the World Meteorological Organization (WMO), which recommends placing sensors over short grass on flat, unobstructed terrain, and positioned away from trees, buildings, or other structures that might shield sensors from full exposure to sunlight and wind (WMO, 2023). While this setup ensures consistency in climate-scale measurements, these requirements are difficult to fulfill over urban environments; and some of them do not necessarily make sense within cities for examining human-centric exposure and impacts at the local scale. Cities are dominated by impervious surfaces and buildings are densely packed, making it challenging to find open unobstructed sites for standard sensor siting. However, capturing the thermal conditions in these areas are essential for understanding the lived experience of heat stress of urban residents in, often, the warmest parts of the city.

To address these limitations, researchers increasingly are turning to non-standard sensors and sensor networks to monitor urban microclimate, particularly temperature, humidity, and heat stress (Muller et al., 2013). Since standard meteorological sensors can be expensive, and multiple sensors are needed to capture the heterogeneity of urban environments, cheaper sensors are often utilized. Various types of low-cost sensors have been and are being used in mobile campaigns (via cars, bikes or on foot) (Shandas et al., 2019; Shi et al., 2021; Wang et al., 2023), stationary sensor networks (Chapman et al., 2015; Fenner et al., 2019; Shi et al., 2021), or as crowdsourced citizen weather station data (Chakraborty et al., 2022; Fenner et al., 2019; Venter et al., 2021; Zumwald et al., 2021).

To enable meaningful comparison both across and within urban environments, however, robust and established methodologies are essential. Here, we explore how the use of low-cost sensors to assess intra-urban variability in heat stress can be vulnerable to inconsistent measurement techniques and sensor biases and determine guidelines and best practices that can ensure meaningful results.

# 2. Methods

- a. Sensor Specification
- In these assessments, we used 41 Kestrel Drop D2 sensors (Kestrel, 2025), measuring AT and RH. Kestrel Drop D2 sensors are factory calibrated at standards of the National Institute

119	of Standards and Technology against traceable reference instruments (Ametek DTI-050
120	Digital Temperature Indicator for AT and Edgetech HT120 Humidity Transmitter for RH)
121	over a controlled measurement range (Nielsen-Kellerman., 2020; -10 to 55 °C for AT and 10
122	to 90% for RH at 25°C). Calibration drift for AT measurements is noted as negligible for the
123	life of the product, and RH is less than 0.25% per year.
124	Kestrel sensors are widely used in urban heat research due to their affordability (~\$109
125	per unit as of August 2025) and ease of deployment in both mobile and stationary
126	configurations. They have been employed across a broad range of applications, including the
127	evaluation of urban heat mitigation strategies, such as street tree canopies (Segura et al.,
128	2022) and cool roofs (Elnabawi et al., 2023) as well as studies assessing heat exposure risks
129	in vulnerable populations (Karanja et al., 2023; Mukhopadhyay & Weitz, 2022). In a
130	comparative validation study of commonly used AT sensors (Bailey et al., 2020), Kestrel
131	sensors exhibited the highest correlation with research grade weather station data.
132	Each of the sensors were housed in a La Crosse Technology passive radiation shield
133	unless stated otherwise to prevent the sensors from heating up in direct sunlight. A benefit of
134	the Kestrel Drop D2 sensor, by comparison to some other low-cost devices, is that the AT
135	probe is suspended using a coiled wire outside of the sensor casing, minimizing the influence
136	of the casing on measurements. Humidity is measured through perforations in the sensor
137	housing which contains a hygrometer (Nielsen-Kellerman., 2020).
138	b. Experimental Setup
139	All sensors were first calibrated in a controlled indoor environment, with the temperature
140	raised to 32 °C. Measurement variance amongst sensors were minimal and within the
141	manufacturer-specified tolerances for accuracy (± 0.5 $^{\circ}$ C for AT, ±2 $^{\circ}$ C for RH) (Nielsen-
142	Kellerman., 2020), confirming there was no unexpected significant internal systemic bias
143	within the sensors. Sensors were then tested outdoors under realistic conditions to determine
144	how various factors can impact the measurements. Configurations are detailed in Fig. 1.

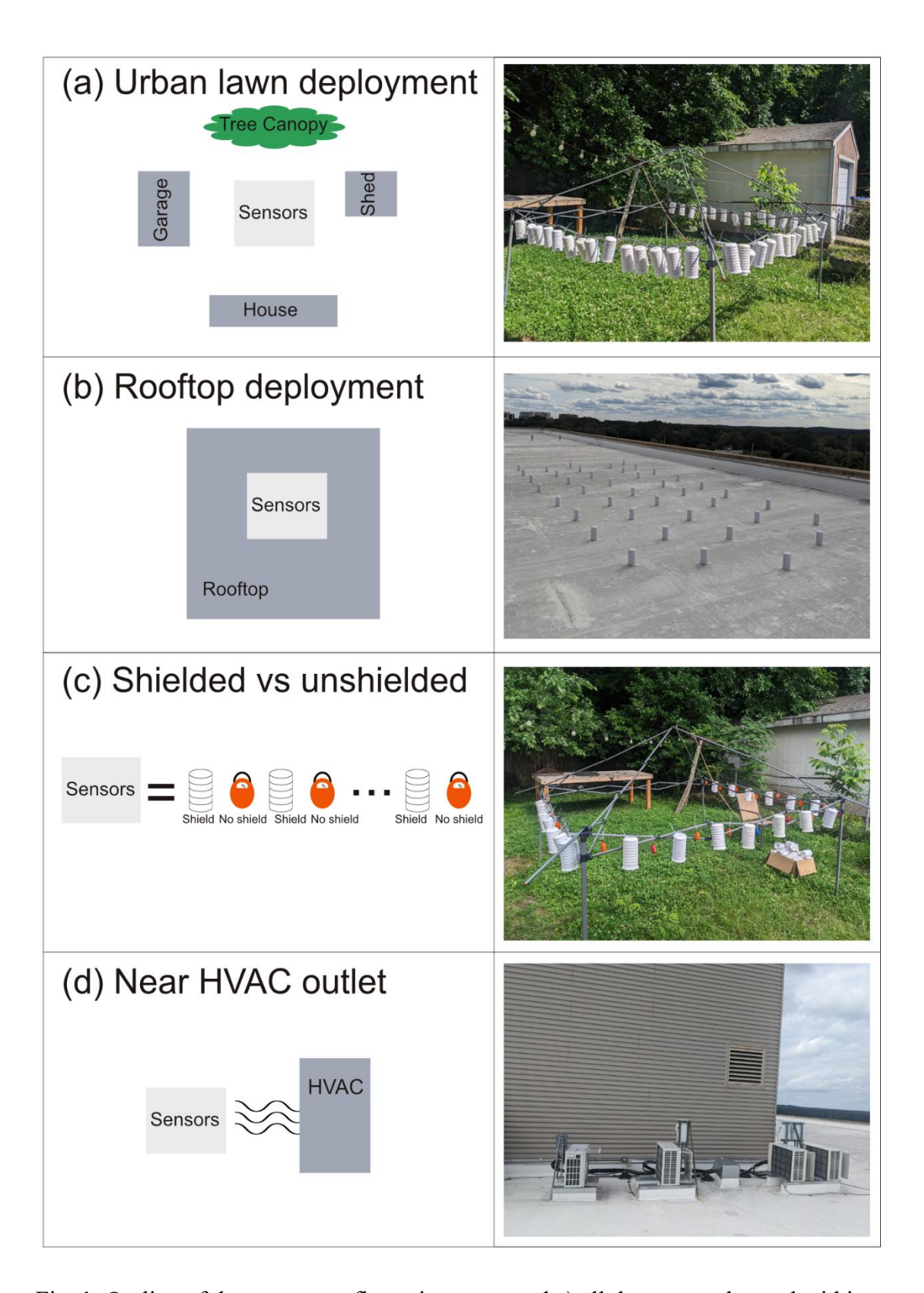


Fig. 1. Outline of the sensor configurations assessed a) all the sensors housed within radiation shields in the urban lawn b) Sensors placed on urban rooftop, c) alternating sensors housed in and outside of radiation shields on the urban lawn location, d) sensors placed 5 - 10 meters from HVAC units on the urban rooftop location. In a separate test, sensors were also placed in a controlled environment with no solar radiation and in different setups within the shield.

153	Sensors recorded data every 10 minutes, and hourly means were calculated as the average
154	within a ±30-minute window to fully represent conditions throughout the hour and reduce the
155	influence of any short lived microclimate fluctuations, in line with current best practices
156	(WMO, 2023). Sensors were deployed at two sites in Chapel Hill, North Carolina, U.S.A., to
157	assess the influence of solar exposure and land cover type: a semi-shaded urban lawn and a
158	fully exposed rooftop. The lawn site consisted of flat terrain with short grass in a suburban
159	residential area, with Local Climate Zone (LCZ) 6, open lowrise (Demuzere et al., 2022). The
160	rooftop was a flat, white painted surface on an 11-story office building (average floor area of
161	2,800 m²), typical of large institutional and office structures in the area (LCZ 5, open
162	midrise), with multiple HVAC units present. Unless specified, sensors were positioned in
163	open areas away from such equipment to minimize localized heating effects. The rooftop
164	location is 1.3 km away from the lawn site and experienced no shading from adjacent
165	buildings.
166	Chapel Hill is characterized as humid subtropical (Koppen Geiger Cfa) (Peel et al., 2007),
167	with precipitation distributed throughout the year. The lawn deployment took place in May,
168	2025 and the rooftop measurements in October, 2024. The lawn sensors took measurements
169	over a period of 16 full days with both clear sky conditions and days of heavy precipitation
170	(Fig. 1a), with the overall mean measured AT of 20.5 °C and RH 79%. The roof top
171	calibration took place over a period of 6 days with clear sky conditions (Fig. 1b) with the
172	period mean AT 14.6 °C, RH 59%. The alternating shielded and unshielded sensors (Fig. 1c)
173	were deployed for 3 days (mean AT 22.5 °C, RH 66% from shielded sensors only).
174	Alternating set ups within the shield (sensors secured to a mounting base in the shield vs
175	suspended on wire) were also deployed for 4 days with a mean AT of 17.2 °C, RH 76%. The
176	rooftop deployment near a localized heat source occurred in late September 2024 with a mean
177	AT of 25.2 °C, RH 72% over a 3-day period (Fig. 1d). Note this reading was likely higher
178	than actual conditions during this time due to the influence of the localized heat source.
179	However, this configuration was specifically intended to reflect real world confounding
180	factors in similar measurement practices, such as from private weather stations set up in
181	backyards.
182	c. Heat Stress Calculations
183	The heat index (HI), representing the feels-like temperature in shaded conditions due to

combined impact of AT and RH, is calculated using results from Steadman (1979) in

alignment with standard US National Weather Service practices. When HI is below 80 °F (26.7 °C), equation (1) is used (with AT in °F).

$$HI = 0.5 \times (AT + 61 + (AT - 68) \times 1.2) + RH \times 0.094$$
 (1)

- For values of HI greater than 80 °F, values are calculated using the Rothfusz equation
- 188 (Rothfusz, 1990), based on a regression of Steadman's table.

$$HI = -42.379 + 2.04901523 AT + 10.14333127 RH - 0.22475541 AT RH$$

$$- 6.83783 \times 10^{-3} AT^{2} - 5.481717 \times 10^{-2} RH^{2}$$

$$+ 1.22874 \times 10^{-3} AT^{2} RH + 8.5282 \times 10^{-4} AT RH^{2}$$

$$- 1.99 \times 10^{-6} AT^{2} RH^{2}$$
(2)

- 189 For high and low values of RH, adjustments are made as per Rothfusz (1990).
- Humidex, another index for moist heat, is also calculated as per the Environment and Climate
- 191 Change Canada (ECCC) (Masterton & Richardson, 1981), in (5) (with AT in °C).

$$Humidex = AT + 0.5555 \times \left(6.11e^{5417.7530 \times \frac{1}{273.15 + TD}} - 10\right)$$
(3)

192 Where TD is dew point temperature (°C).

## 193 **3. Results**

- 194 a. The diurnal cycle of standard error
- A known challenge with AT measurement is the presence of microclimate variability
- within a small area, even in an idealized setup in an isolated area. In urban areas, land cover,
- shading, wind disruption, and anthropogenic heat amplify these effects, making localized
- variability a key concern for sensor networks that prioritize spatial coverage. Even when
- placed in a radiation shield, solar and longwave radiation can result in measurement
- variability across sensors (Bell et al., 2015).
- Here, we analyzed the standard error amongst daily hourly mean sensor readings at each
- deployment location. The variance amongst sensor readings in the small deployment areas
- shows a clear diurnal cycle, highlighting key times of day where spatial comparisons should
- be made with caution. Of note, at night (defined as periods when incoming solar radiation

was zero using ERA5-Land reanalysis data (Muñoz Sabater, 2019)), standard error amongst sensors is minimal, but greatly increases during daytime hours (Fig. 2), when the atmosphere is less stable and radiation can impact sensor accuracy.

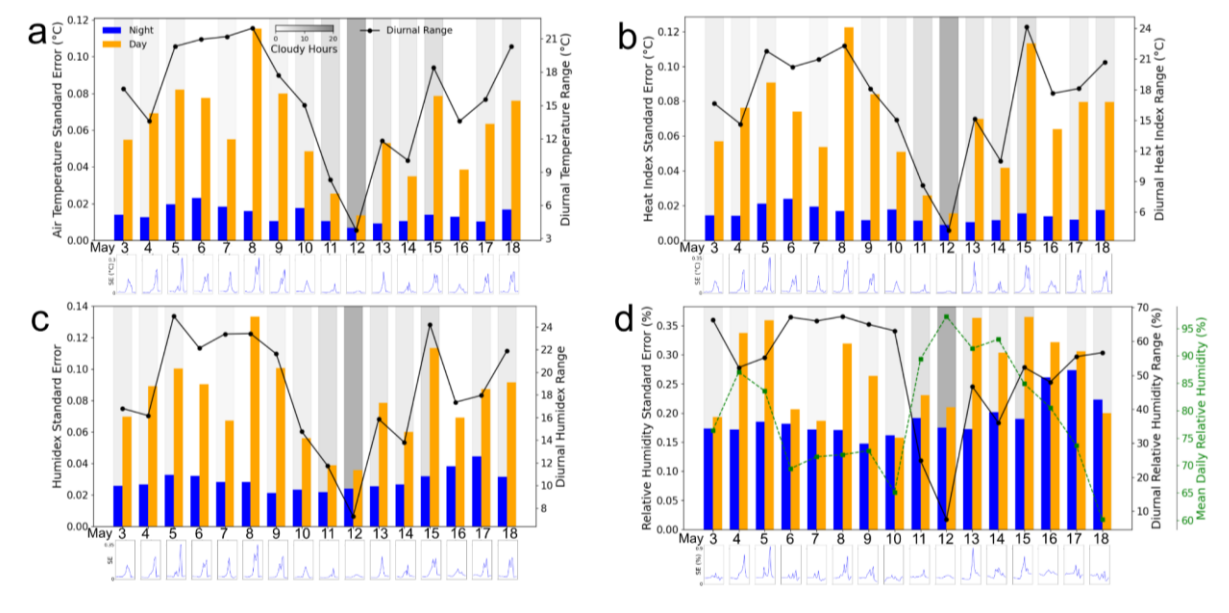


Fig. 2. Standard error (primary axis) and temperature range (secondary axis) for sensors in an urban lawn. Small daily plots beneath bars show the diurnal cycle of standard error for each date.

The magnitude of the AT daytime error is highly correlated with the diurnal temperature range, with Pearsons's correlation coefficient (r) of 0.85 (Fig A1a, Table A1) during a 15-day period in the urban lawn setting (Fig. 2a). The correlation remains high for sensors deployed on an unshaded rooftop for a 6-day period (r = 0.98) (Fig. A1). Nighttime correlations also show a similar relationship (r = 0.79) over urban lawn; 0.93 for rooftop). Figures 2 and A2 additionally show the diurnal pattern of standard error for each individual day. During daytime hours, differences between the sensor AT measurements (Fig. 2a) tend to be the most prominent in transitional periods when AT is rising or falling rapidly. This result is in line with expectations based on guidance from the WMO, who do not recommend taking urban AT surveys close to sunrise or sunset as rapid changes in weather variables at these times make spatial comparisons difficult.

In the rooftop setting, over an impervious surface, diurnal RH range and measurement standard error are correlated (r = 0.80). However, in the lawn scenario (Fig. 2c), a relationship is only seen after controlling for the mean RH, when larger diurnal (meanadjusted) RH ranges are positively correlated with daytime standard error in measurements (r = 0.49) (Fig. A1, Table A1). During the night, similar patterns emerged, with no correlations

found between measurement standard error and diurnal RH range over grass, but strong positive correlations in the rooftop location (Fig. 1b, Table A1). This contrast indicates that water retention and evapotranspiration processes in grass may alter localized RH variability. While the magnitude of RH error over both surfaces is similar, different processes appear to dominate depending on the surface type.

HI inherits any uncertainty present in the two input variables. This issue is visible within its measurement standard error (Fig. 2b), which is amplified in comparison to AT (by 4.7%). The general relationship remains similar to that of AT, with a strong correlation between measurement standard error and diurnal cycle during the day (lawn r = 0.86, rooftop r = 0.97) and night (lawn r = 0.68, rooftop r = 0.90) (Fig. A1, Table A1).

To evaluate how much of the observed standard error could be attributed to controllable, sensor or position specific bias, a regression-based calibration was performed by comparing each sensor's readings to the overall mean and applying the resulting correction equations to a separate test period. However, neither sensor ID nor position consistently predicted bias magnitude or direction, and calibration adjustments often increased the spread of measurements. These findings suggest that external environmental factors, particularly diurnal temperature range (Fig. 2), are more influential than intrinsic sensor behavior. For daytime spatial comparisons, when variability is greatest, observed temperature differences must exceed the background cross-sensor variability to be meaningful.

#### b. Radiation Shielding

AT measurements taken without radiation shielding exhibit a daytime warm bias compared to those from shielded sensors (Fig. 3, Fig. A3). This discrepancy is most pronounced during the warmest hours of the day (from 1pm until 6pm), when solar radiation directly heats the sensor casing, causing it to register artificially elevated temperatures. In contrast, during nighttime (between ~10pm and ~6am), when solar radiation is absent, the mean temperatures recorded by both shielded and unshielded sensors converge.

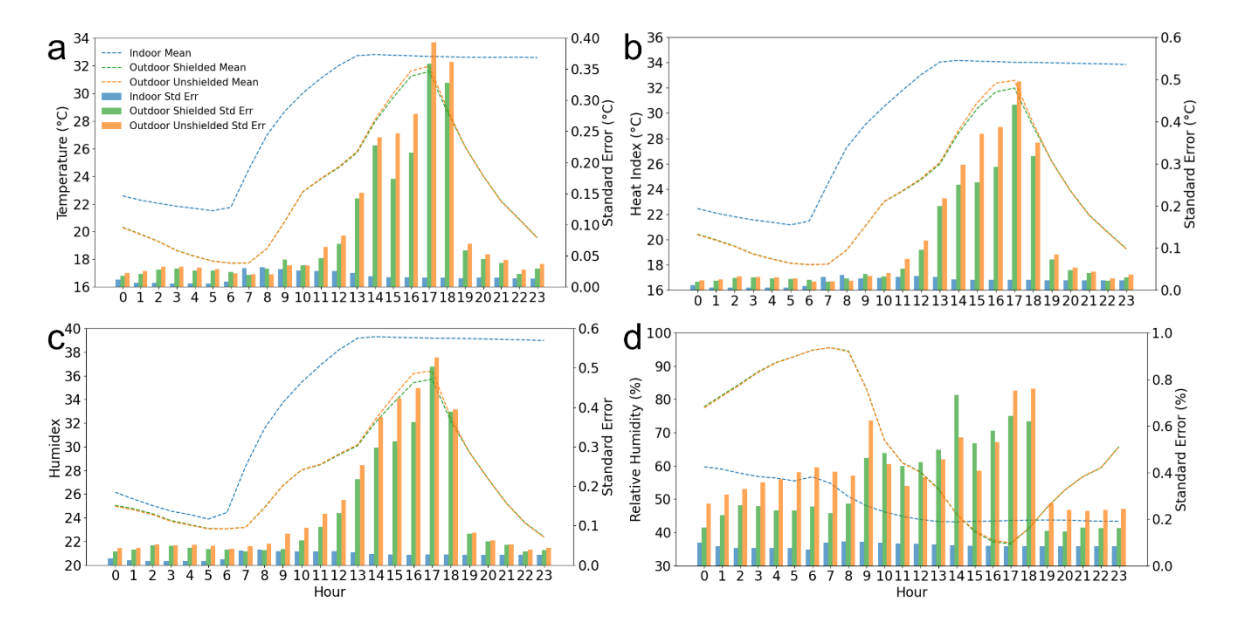


Fig. 3. Comparisons of standard error across sensors when shielded, unshielded and in absence of solar radiation. Hourly mean values for a) AT, b) HI, c) Humidex and c) RH, (lines, primary axis) and standard error (bars, secondary axis) from sensors placed indoors (Fig. 1e) and in an urban lawn setup with and without radiation shields (Fig. 1c).

While shields are an effective way of decreasing the interference of solar radiation, they are not 100% effective. Radiation shields and sensor casing also can absorb and store radiant heat (longwave radiation), particularly if they are not ventilated, leading to inflated readings. This shielding versus ventilation tradeoff with unaspirated, passive radiation shields means there can be a lag in the AT readings during temperature rise due to the lack of ventilation. The impact of ventilation is potentially apparent on the May 20 result (Fig. A3a), where the standard error for shielded briefly exceeds unshielded sensors.

For both HI and Humidex, unshielded sensors consistently overestimate values during the warmest afternoon hours (Fig. 3). This bias is primarily driven by artificially elevated AT readings caused by direct solar exposure. In contrast, the effect of radiation shielding on RH is minimal, with values remaining similar between shielded and unshielded sensors, and no consistent pattern of divergence is observed. Standard error magnitudes for RH can vary with or without shielding, but they do not follow a clear diurnal pattern, nor are they as strongly affected by solar radiation as AT observations. Of note, however, is that the calibration experiment took place over days with no precipitation. The signal of RH standard errors appears more in the Humidex than HI observations, with evening (9pm and 10pm) high standard errors in RH (Fig. 3). This is because Humidex is more sensitive to RH than HI (Chakraborty et al., 2022; Sherwood, 2018).

As an aside, different set ups within the radiation shield were also examined, and no discernable difference in standard error was found from suspending the sensors in the shield in comparison to securing the sensor at the bottom of the shield on a mounting base.

# c. Measurement Frequency

Standard meteorological practice involves taking measurements every 5 minutes, which are then aggregated to an average to represent hourly conditions. This can highlight outliers and gives a full representation of the conditions during the hour. Using hourly means reduced AT standard error compared to single-point measurements (Fig. 4a), while single measurements also produced a larger diurnal range. A similar increase in the range of measurements logged is seen for RH (Fig.4d), which again are inherited in both HI and Humidex (Fig. 4bc).

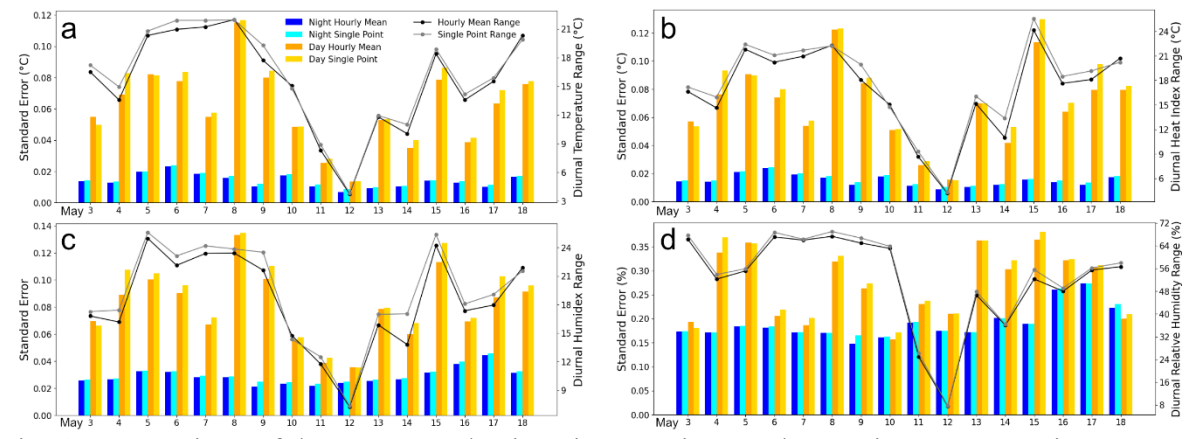


Fig. 4. Comparison of data generated using six ten-minutes observations versus using a single, top of the hour measurement. Both the differences in standard error (bars) and the diurnal range (lines) are considered for a) AT, b) HI, c) Humidex, d) RH.

## d. Sensor Placement

A sensor's immediate surroundings can have a profound effect on the accuracy and reliability of micrometeorological observations. In urban settings, proximity to anthropogenic heat sources such as air conditioning (AC) outlets, vents, or machinery can significantly bias measurements, leading to misleading spatial patterns if not properly accounted for. To quantify the impact of such localized heat sources, we conducted a comparison with sensors deployed on the rooftop, by deploying sensors in a location near HVAC units for a 3 day period (Fig. A6). The daytime standard error between sensors was 0.76 °C AT and 2.3% RH, over seven (AT) and approaching ten (RH) times higher than the rooftop sensor placement

away from the outlets (0.10 °C, 0.25%). A similar trend was observed at night, with a
standard error of 0.24 °C AT and 2.7% RH near the HVAC unit compared to just 0.02 °C and
0.1% RH in the interference-free setting. The average diurnal temperature range during both
deployments was nearly identical (20.6 °C near unit vs. 20.4 °C for the isolated sensor),
confirming that the increase in AT variability was not due to broader atmospheric conditions.
RH was higher during the HVAC deployment (73% versus 59%), which may have
additionally inflated standard error, as rainfall occurred during the final day (Fig. A6).

## 4. Discussion and Conclusion

There is a need to establish clear guidelines and quality control measures for making robust intra-urban heat stress comparisons when using low-cost sensors. Outdoor deployments introduce a range of challenges not captured in standard testing environments, yet most AT sensor calibrations are conducted under controlled conditions (Abdinoor et al., 2025). Whereas previous studies have primarily emphasized validating low-cost sensors against a research-grade reference instrument (Fenner et al., 2021; Meier et al., 2017), our focus is on examining variability among sensors themselves. The goal is to assess their suitability for capturing spatial differentials within the same sensor type, rather than prioritizing absolute accuracy relative to a reference.

Our findings suggest environmental factors and methodological choices introduce substantial variability that can undermine the accuracy of both spatial comparisons and estimates of UHI and UDI magnitude if not carefully accounted for. We demonstrate that the performance of AT and RH sensors can degrade significantly when employed in outdoor field conditions, as other studies confirm (Yamamoto et al., 2017; Yulizar et al., 2023), with crowdsourced sensors in particular shown to overestimate AT and underestimate RH (Chakraborty et al., 2022). Although we did not observe calibration drift in RH measurements during our deployments, such drift has been reported as a potential issue in other studies (da Cunha, 2015). These results highlight the importance of conducting sensor validation and calibration under real-world, field-based conditions to ensure reliability and accuracy of environmental monitoring, particularly in heterogeneous urban settings.

#### a. Radiation Shielding

Radiation shields improve AT accuracy by preventing sensor probes and casings from heating in direct sunlight, which otherwise drives them out of equilibrium with ambient air

335	(da Cunha, 2015). Solar radiation is a dominant confounding factor for measurement
336	accuracy, with studies identifying the most accuracy reductions in AT during periods of high
337	radiation (Sun et al., 2015; Yamamoto et al., 2017), also seen here for AT, HI and Humidex
338	(Fig. 2, Fig. A2). This establishes the necessity of using some form of radiation shielding for
339	outdoor measurements. This is already a requirement for standard meteorological
340	measurements but sometimes avoided due to cost and logistical issues in urban environments
341	This is a major issue for citizen weather stations (Alerskans et al., 2022; Bell et al., 2015;
342	Cornes et al., 2020; Jenkins, 2014). Unshielded sensors recorded higher daytime temperature
343	during the hottest hours of the day on all occasions (Fig. 3), artificially inflating daily
344	maximum temperatures, potentially overestimating UHI magnitudes, and spatial variability
345	across parts of the city with different amounts of shading. Failure to shield sensors may also
346	interfere with assessments of cooling measures such as due to tree canopy or shading
347	structures, as comparison sensors exposed to direct sunlight will show inflated ATs.
348	Additionally, adequate shielding is important for accurate RH measurements, which require
349	the sensor to remain dry and, as RH is derived using AT, artificially high ATs will lead to
350	underestimated RH (da Cunha, 2015).
351	In addition to absolute radiation levels, rapid changes in solar radiation, such as those
352	occurring around sunrise and sunset, appear to exacerbate measurement standard errors.
353	Yamamoto et al (2017) noted that abrupt shifts in solar intensity led to large fluctuations in
354	sensor readings. Young et al (2014) similarly finds the largest errors in sensor readings occur
355	around sunrise, potentially due to two mechanisms; enhanced radiation errors caused by the
356	low solar angle, and inadequate ventilation in radiation shields leading to heat buildup and
357	stagnant air. Notably, these errors varied by deployment, suggesting limited generalizability.
358	This issue is reflected in our own findings, where standard error was not consistent in all the
359	tests done (Fig. 2), and therefore difficult to correct for.
360	b. Landcover and Surroundings

362

363

364

365

366

Other environmental factors, such as land cover, can further influence sensor performance. Nan et al (2025) demonstrated that AT calibration equations optimized for specific land cover types (e.g., grass, forest, synthetic turf) yielded varying levels of accuracy, indicating that local surface characteristics can influence sensor behavior and that a one-size-fits-all calibration may not be effective across diverse urban landscapes. Our findings also highlight that RH presents distinct challenges. Because sensor-measured RH is

derived from AT, it is indirectly affected by radiation, but its measurement variability is also closely tied to land cover types. In our deployments, grass cover dampened the correlation between diurnal range and RH error, whereas the impervious rooftop location, lacking surface moisture, exhibited stronger correlations (Fig. A2, Table A1).

The need for metadata on sensor surroundings has long been considered an important consideration in urban micrometeorology (Stewart, 2011). Sensors placed near localized heat sources (Fig. 1d) exhibited highly inflated standard errors over seven times greater in AT and almost ten times for RH than those in undisturbed locations (Fig. A6), although it is possible RH variability is further increased due to rainfall. This result highlights the need for careful siting away from such influences and recording of sensor surroundings. Simple metadata fields such as proximity to buildings or mechanical systems could help screen for potential problematic sensors and improve confidence in spatial comparisons. In crowdsourced networks, where detailed metadata is often lacking, this emphasizes the need for anomaly detection and quality control (Fenner et al., 2021; Napoly et al., 2018).

# c. Measurement Frequency

Comparisons between single point and hourly averaged measurements showed that averaging reduces standard error (Fig. 4), resulting in more stable spatial comparisons. Low sampling frequencies are more vulnerable to transient effects, such as passing clouds, which can distort results. This has direct implications for studies where, due to storage capacity and retrieval time, sampling frequency is low, as well as transect-based studies that rely on single point observations (Meier et al., 2017; Romero Rodríguez et al., 2020; Shandas et al., 2019; Wang et al., 2023). Although traverse measures have the advantage they do not have to deal with inter-sensor comparison, the utilized sensors must have a rapid response time, particularly if the traverse is done by car (WMO, 2023). While such methods are valuable for spatial coverage and avoid the more time consuming and costly approach of a static sensor network, they should be interpreted with care.

#### d. Managing sensor variability

We find a significant role of the diurnal cycle in shaping measurement standard error. Standard error was lowest at night, when atmospheric conditions are more stable and there is no solar radiation. During the daytime, variability amongst sensor measurements increases, particularly during periods of rapid heating or cooling. This difference is reflected in the

strong correlation of standard error with the diurnal temperature range. Even with radiation shielding, sensors may respond inconsistently to radiative heating due to differences in passive ventilation. Unaspirated shields can retain heat and minor differences in airflow across sensors can lead to variability in readings, meaning the thermal response of each sensor becomes more susceptible to local conditions, contributing to increased measurement divergence during periods of strong solar forcing. As a result, spatial comparisons are more robust at night or for days when the diurnal temperature range is relatively small. However, given the importance of heat on human health and comfort during the daytime when temperatures are warmest, adding 'guardrails' to reflect this discrepancy can help. Diurnal temperature range, for example, may serve as a useful proxy for expected variability and could help establish confidence intervals for spatial comparisons of heat stress.

Since Chapel Hill is a humid climate, both AT and RH are important components of the moist heat stress burden, and thus its measurement error. In drier climates, AT typically dominates heat stress variability; so errors in RH would have a smaller impact. Additionally, the relatively low wind speeds typical of Chapel Hill limit airflow around sensors, whereas windier locations, such as coastal cities, may benefit from enhanced natural ventilation. We should also note here that different moist heat stress indices have different sensitivity to AT and RH, with relevance for cross-sensor variability depending on the index chosen (Chakraborty et al., 2022; Sherwood, 2018).

Based on our findings, we recommend the following best practice for low-cost urban sensor monitoring;

- 1. Use radiation shields to reduce exaggerated daytime heating.
- 2. Exercise caution when making comparisons during times of rapid heating or cooling add confidence intervals into any spatial comparisons.
- 3. Take multiple measurements over an hour and use the average rather than a single observation.
  - 4. Document sensor surroundings and deploy them away from potential anthropogenic heat sources.

As cities around the world increasingly aim to better map urban temperature and build policies to mitigate and adapt to extreme heat, the reliability of such measures is essential. Low-cost sensors, when used properly, can play a powerful role in identifying potential disparities in urban heat and better quantify the efficiencies of targeted intervention and

430	mitigation efforts. By identifying key guidelines for best practices to minimize cross-sensor
431	variability due to localized artifacts or measurement noise, and offering practical, evidence-
432	based guardrails that can aid spatial comparisons, this study contributes to the development of
433	standardized urban temperature monitoring frameworks.
434	
435	Acknowledgments.
436	This work was supported in part by a grant/cooperative agreement from the National
437	Aeronautics and Space Administration (NASA) under Award No 80NSSC24K0505;22-
438	IDS22-0146.
439	
440	Data Availability Statement.
441	The dataset supporting this study, "Biases due to widespread use of low-cost sensors for
442	urban heat stress assessments (dataset)", is openly available on Zenodo at:
443	https://doi.org/10.5281/zenodo.17180023
444	APPENDIX
115	Appendix A: Additional Figures

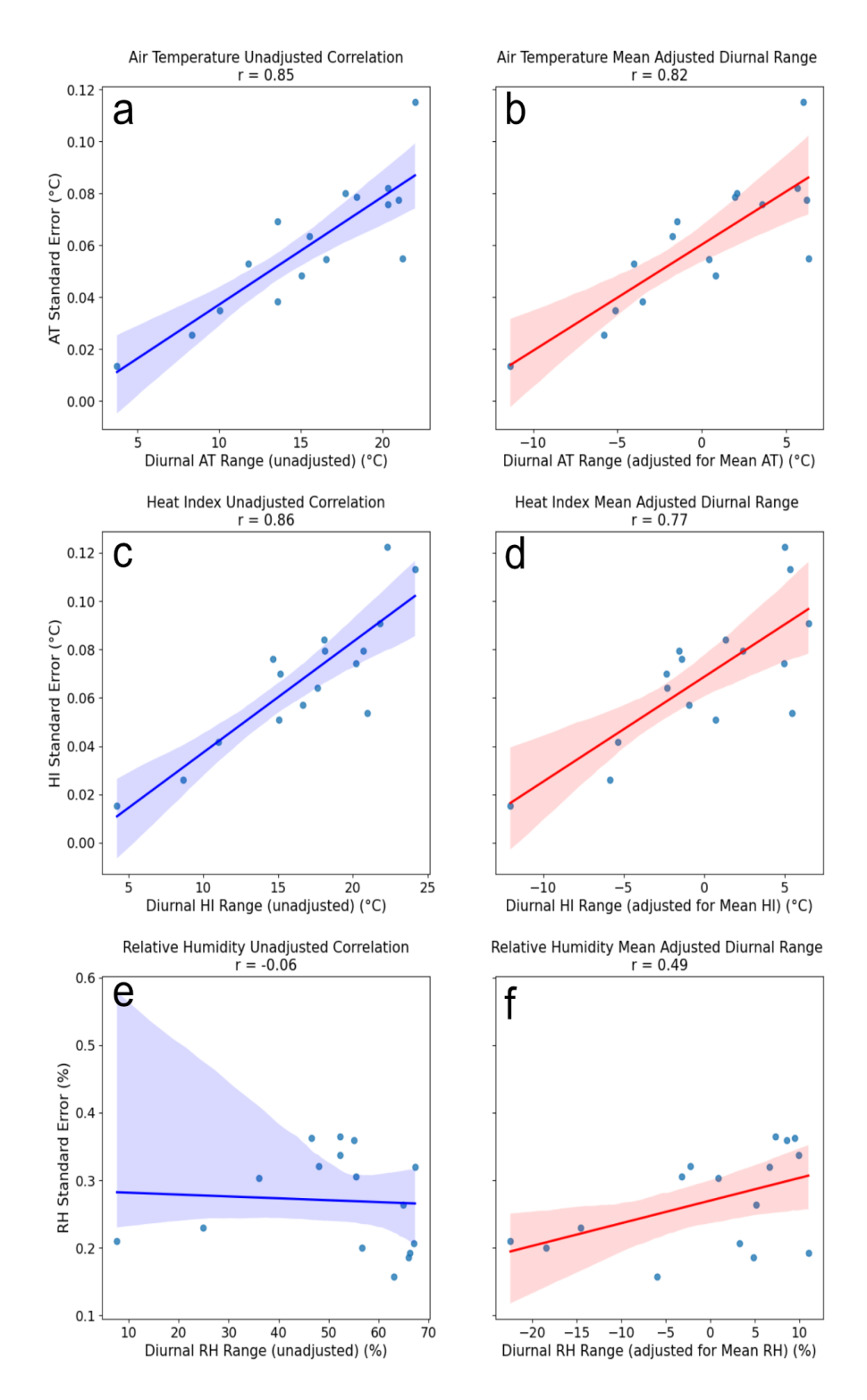


Fig. A1: Correlations between diurnal ranges and measurement standard error. Figures show the 'raw' unadjusted correlations, then partial correlations where diurnal range is adjusted for by the measurement mean by creating a linear regression where x= measurement mean and y= diurnal range. The residuals of the fit are taken as the adjusted diurnal range. Also shown on the figure is a least squares regression is plotted with a 95% confidence interval (blue for unadjusted, red for adjusted fits). Shown in figure is a) AT unadjusted, b) AT adjusted, c) heat index unadjusted, d) heat index adjusted, e) RH unadjusted, f) RH adjusted.

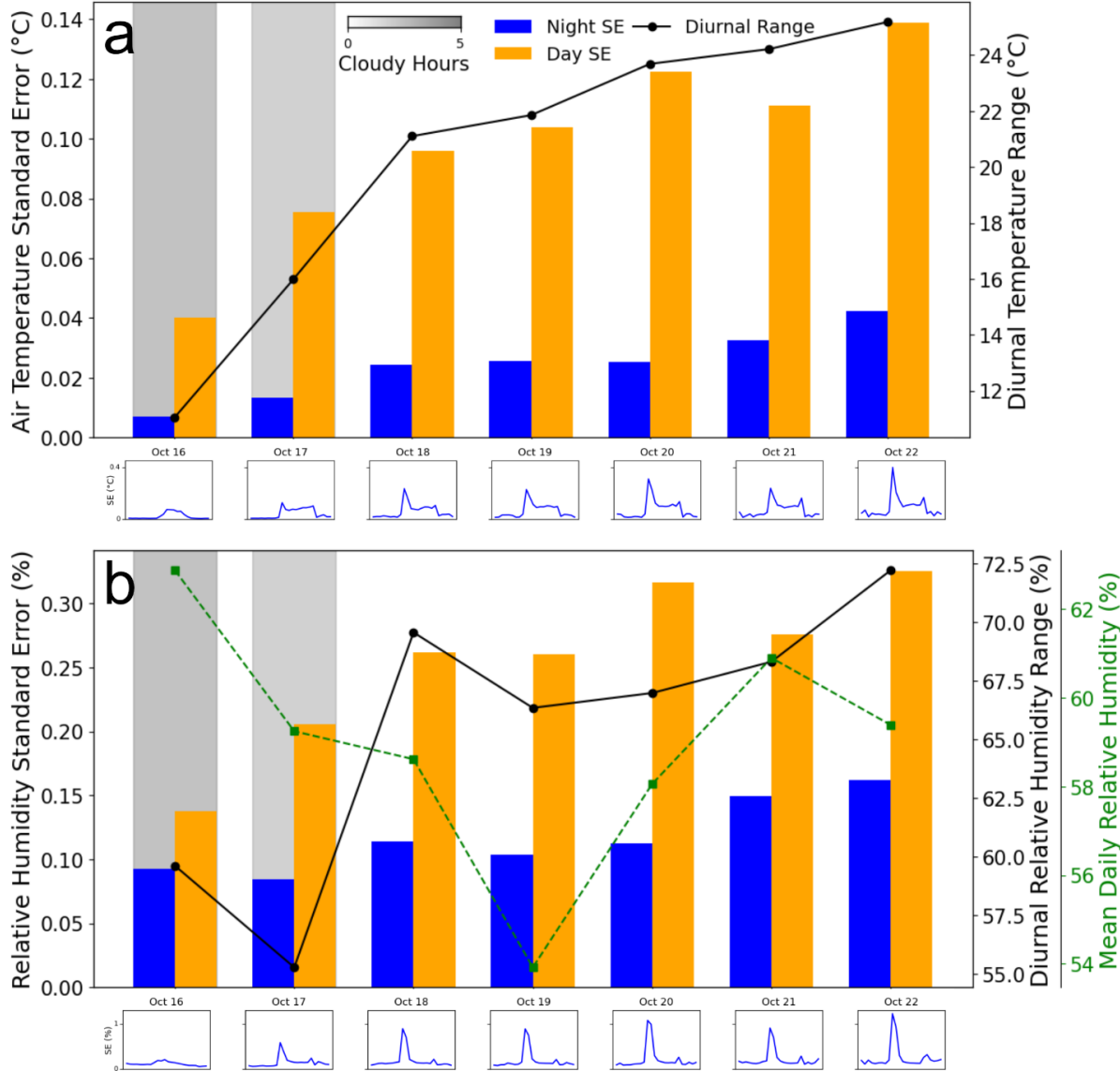


Fig. A2 a) AT and b) RH Standard error (primary axis) and diurnal range (secondary axis) for sensors on an unshaded rooftop. Small daily plots beneath bars show the diurnal cycle of standard error for each date.

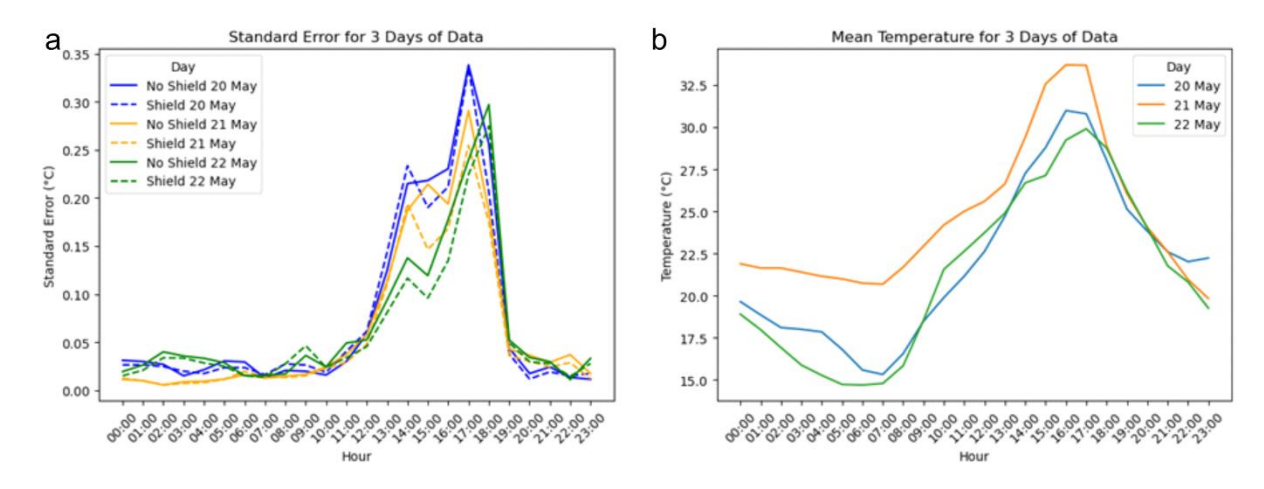
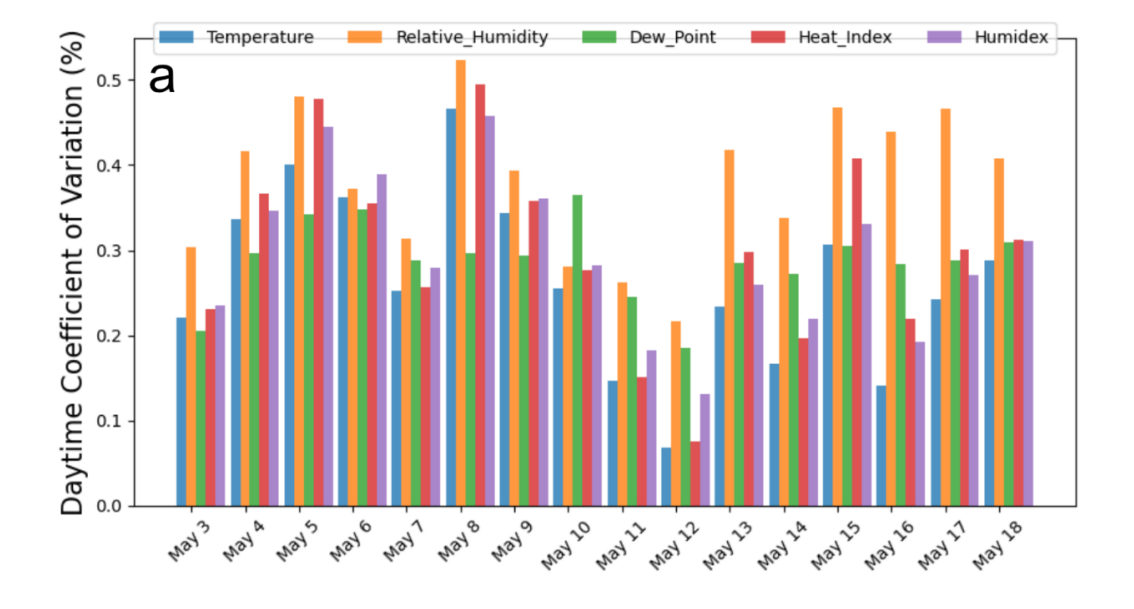


Fig. A3: a) Standard error for individual days sensors were tested in alternating shielded and unshielded setups, with b) the mean AT diurnal cycle for each of the days.



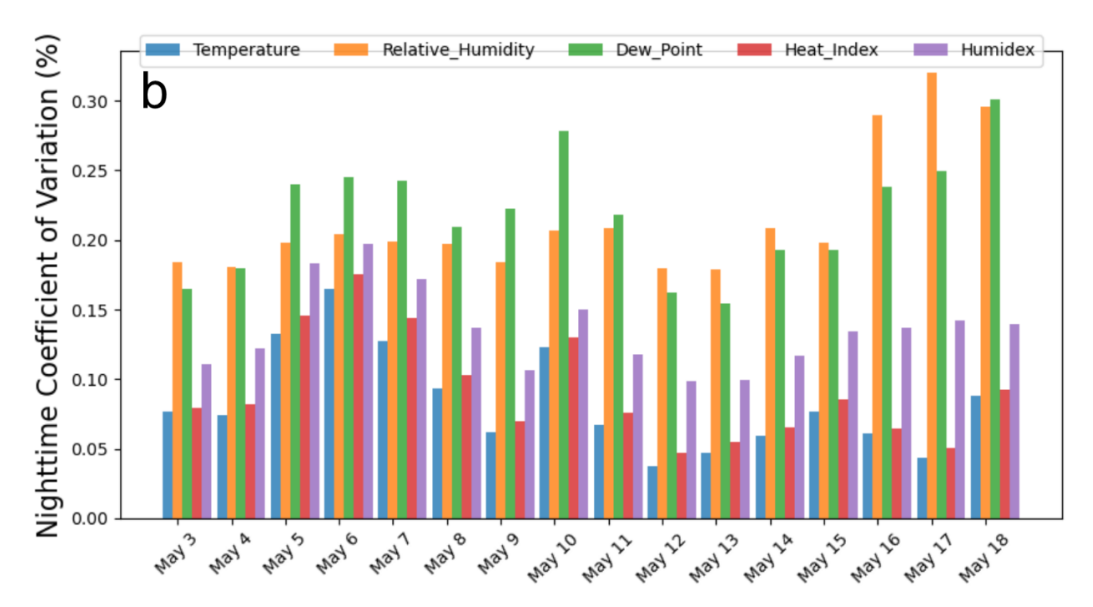


Fig. A4: Coefficient of variation for each of the heat stress measurements for a) daytime measurements, and b) nighttime. Coefficient of variation is defined as the measurement standard error as a percentage of the mean of the measurement.

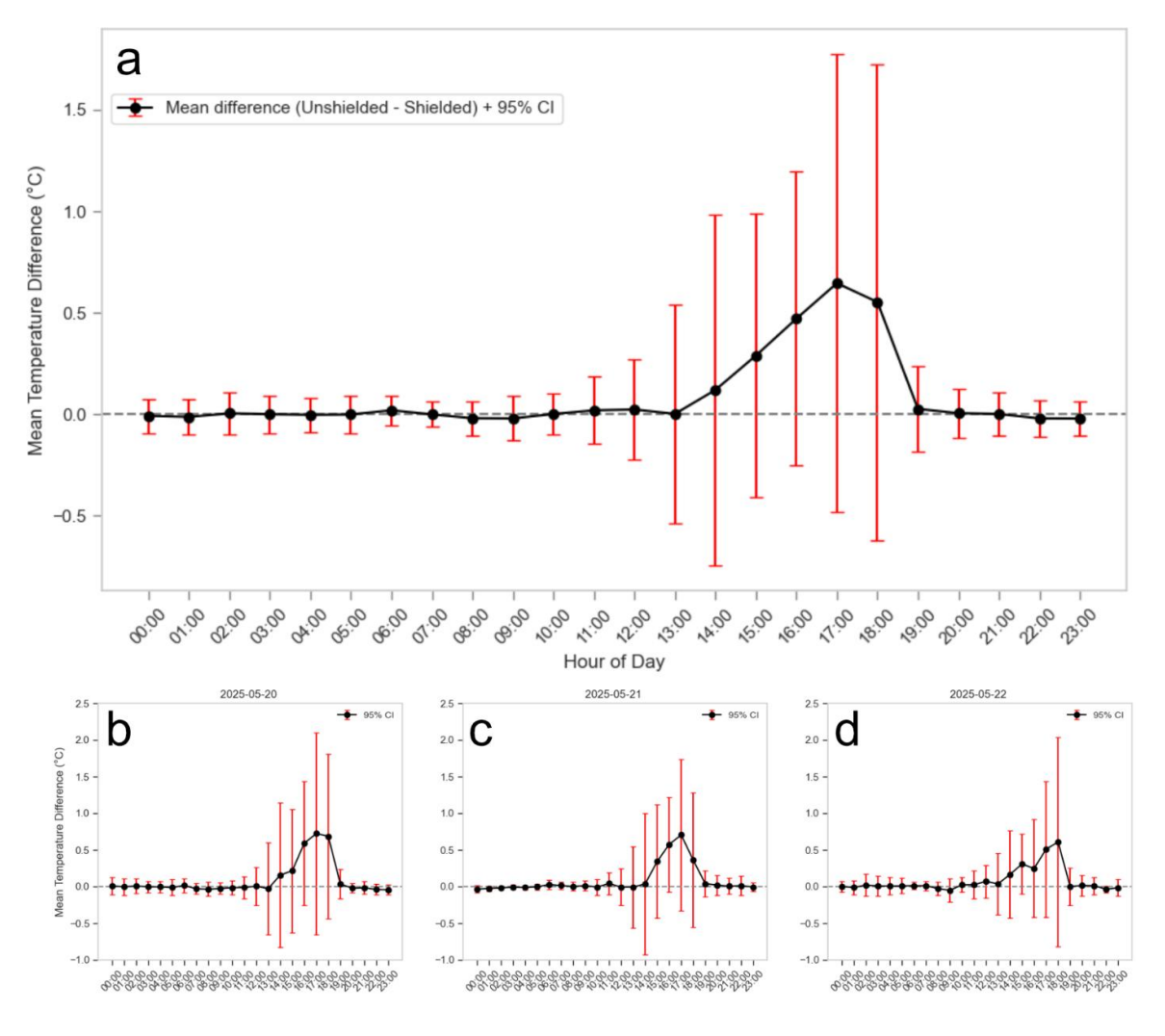


Fig. A5: Mean Temperature Difference between shielded and unshielded sensors with 95% confidence intervals for shielding differences, calculated using differences between adjacent sensor pairs. Figure shows a) average differences over a 3-day period, and differences on individual days b) 2020-05-20, c) 2020-05-21, d) 2020-05-22.

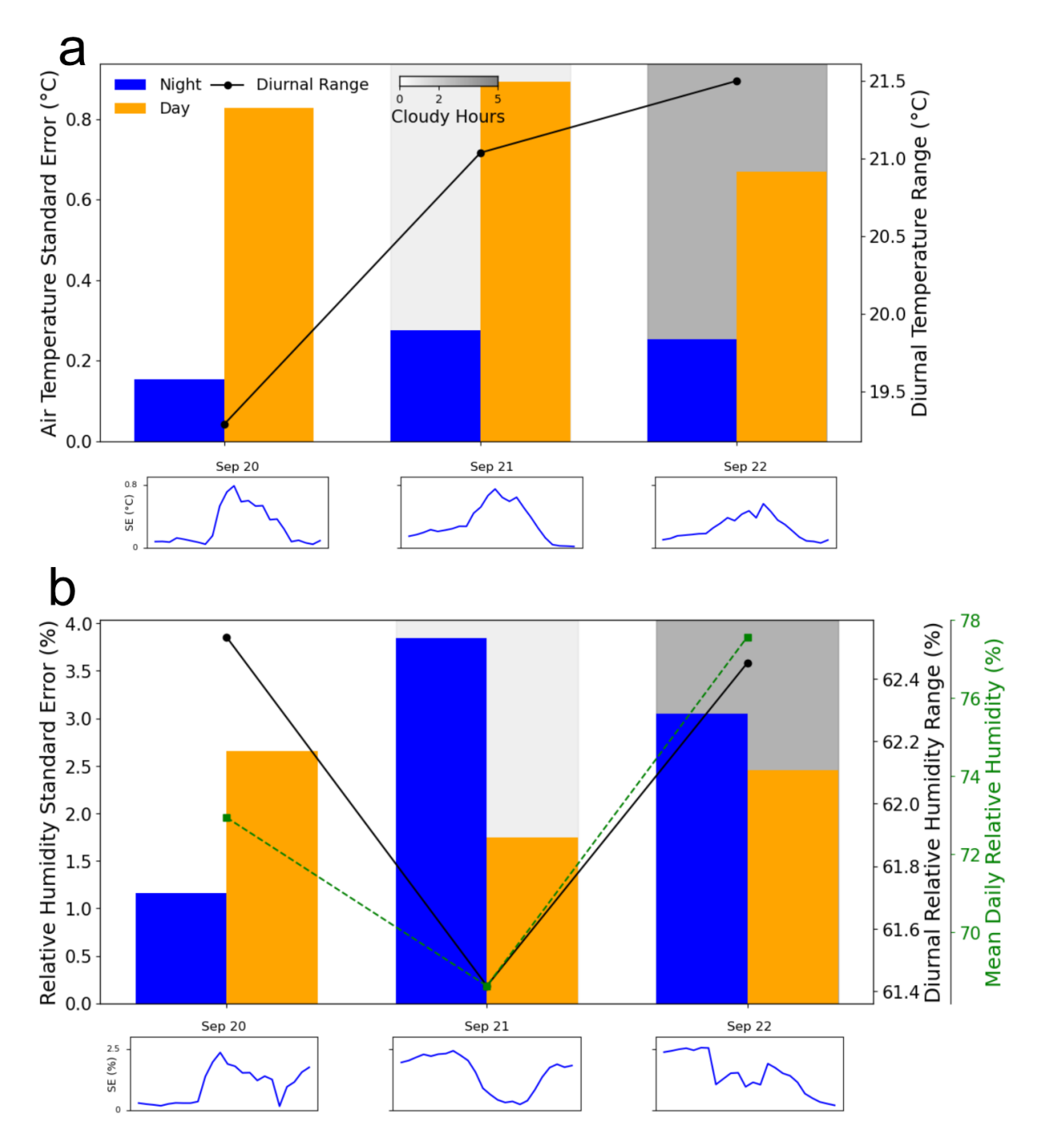


Fig. A6: a) AT and b) RH Standard error (primary axis) and diurnal range (secondary axis) for sensors placed near an external heat source (HVAC unit) on an unshaded rooftop. Small daily plots beneath bars show the diurnal cycle of standard error for each date.

	Measurement	Unadjusted correlation		Mean adjusted correlation	
		Lawn	Rooftop	Lawn	Rooftop
Day	AT	0.85	0.97	0.82	0.36
	НІ	0.86	0.97	0.77	0.51
	Humidex	0.83	0.97	0.82	0.39
	RH	-0.065	0.80	0.49	0.70
Night	AT	0.79	0.93	0.85	0.26
	НІ	0.68	0.90	0.82	0.25
	Humidex	0.35	0.90	0.34	0.22
	RH	-0.13	0.83	-0.29	0.87

Table A1. Pearson's Correlation Coefficients between measurement standard error and diurnal range or mean-adjusted diurnal range. Coefficients which are significant based on a threshold p<0.05 are highlighted in bold.

500	
501	REFERENCES
502	Abdinoor, J. A., Hashim, Z. K., Horváth, B., Zsebő, S., Stencinger, D., Hegedüs, G., Bede,
503	L., Ijaz, A., & Kulmány, I. M. (2025). Performance of Low-Cost Air Temperature
504	Sensors and Applied Calibration Techniques—A Systematic Review. Atmosphere,
505	16(7), 842. https://doi.org/10.3390/atmos16070842
506	Alerskans, E., Lussana, C., Nipen, T. N., & Seierstad, I. A. (2022). Optimizing Spatial
507	Quality Control for a Dense Network of Meteorological Stations.
508	https://doi.org/10.1175/JTECH-D-21-0184.1
509	Bailey, E., Fuhrmann, C., Runkle, J., Stevens, S., Brown, M., & Sugg, M. (2020). Wearable
510	sensors for personal temperature exposure assessments: A comparative study.
511	Environmental Research, 180, 108858. https://doi.org/10.1016/j.envres.2019.108858
512	Bell, S., Cornford, D., & Bastin, L. (2015). How good are citizen weather stations?
513	Addressing a biased opinion. Weather, 70(3), 75–84.
514	https://doi.org/10.1002/wea.2316
515	Chakraborty, T., Newman, A. J., Qian, Y., Hsu, A., & Sheriff, G. (2023). Residential
516	segregation and outdoor urban moist heat stress disparities in the United States. One
517	Earth, 6(6), 738–750. https://doi.org/10.1016/j.oneear.2023.05.016
518	Chakraborty, T., Venter, Z. S., Qian, Y., & Lee, X. (2022). Lower Urban Humidity
519	Moderates Outdoor Heat Stress. AGU Advances, 3(5), e2022AV000729.
520	https://doi.org/10.1029/2022AV000729
521	Chapman, L., Muller, C. L., Young, D. T., Warren, E. L., Grimmond, C. S. B., Cai, XM., &
522	Ferranti, E. J. S. (2015). The Birmingham Urban Climate Laboratory: An Open
523	Meteorological Test Bed and Challenges of the Smart City. <i>Bulletin of the American</i> 26

524	Meteorological Society, 96(9), 1545–1560. https://doi.org/10.1175/BAMS-D-13-
525	00193.1
526	Cornes, R. C., Dirksen, M., & Sluiter, R. (2020). Correcting citizen-science air temperature
527	measurements across the Netherlands for short wave radiation bias. Meteorological
528	Applications, 27(1), e1814. https://doi.org/10.1002/met.1814
529	da Cunha, A. R. (2015). Evaluation of measurement errors of temperature and relative
530	humidity from HOBO data logger under different conditions of exposure to solar
531	radiation. Environmental Monitoring and Assessment, 187(5), 236.
532	https://doi.org/10.1007/s10661-015-4458-x
533	Demuzere, M., Kittner, J., Martilli, A., Mills, G., Moede, C., Stewart, I. D., van Vliet, J., &
534	Bechtel, B. (2022). A global map of local climate zones to support earth system
535	modelling and urban-scale environmental science. Earth System Science Data, 14(8),
536	3835-3873. https://doi.org/10.5194/essd-14-3835-2022
537	Elnabawi, M. H., Hamza, N., & Raveendran, R. (2023). 'Super cool roofs': Mitigating the
538	UHI effect and enhancing urban thermal comfort with high albedo-coated roofs.
539	Results in Engineering, 19, 101269. https://doi.org/10.1016/j.rineng.2023.101269
540	Fenner, D., Bechtel, B., Demuzere, M., Kittner, J., & Meier, F. (2021). CrowdQC+—A
541	Quality-Control for Crowdsourced Air-Temperature Observations Enabling World-
542	Wide Urban Climate Applications. Frontiers in Environmental Science, 9, 720747.
543	https://doi.org/10.3389/fenvs.2021.720747
544	Fenner, D., Holtmann, A., Meier, F., Langer, I., & Scherer, D. (2019). Contrasting changes of
545	urban heat island intensity during hot weather episodes. Environmental Research
546	Letters, 14(12), 124013. https://doi.org/10.1088/1748-9326/ab506b

547	Hersbach, H., Bell, B., Berrisford, P., Hirahara, S., Horányi, A., Muñoz-Sabater, J., Nicolas,
548	J., Peubey, C., Radu, R., Schepers, D., Simmons, A., Soci, C., Abdalla, S., Abellan,
549	X., Balsamo, G., Bechtold, P., Biavati, G., Bidlot, J., Bonavita, M., Thépaut, J.
550	(2020). The ERA5 global reanalysis. Quarterly Journal of the Royal Meteorological
551	Society, 146(730), 1999–2049. https://doi.org/10.1002/qj.3803
552	Hsu, A., Sheriff, G., Chakraborty, T., & Manya, D. (2021). Disproportionate exposure to
553	urban heat island intensity across major US cities. Nature Communications, 12(1),
554	2721. https://doi.org/10.1038/s41467-021-22799-5
555	Jenkins, G. (2014). A comparison between two types of widely used weather stations.
556	Weather, 69(4), 105–110. https://doi.org/10.1002/wea.2158
557	Karanja, J., Vieira, J., & Vanos, J. (2023). Sheltered from the heat? How tents and shade
558	covers may unintentionally increase air temperature exposures to unsheltered
559	communities. Public Health in Practice, 6, 100450.
560	https://doi.org/10.1016/j.puhip.2023.100450
561	Kestrel. (2025). [Kestrel DROP D2 Tiny Temperature & Humidity Data Logger]. Nielsen-
562	Kellerman. https://kestrelmeters.com/kestrel-drop-d2-humidity-logger
563	Li, J., Zhan, W., Chakraborty, T. C., Liu, Z., Du, H., Liao, W., Luo, M., Li, L., Miao, S., Fu,
564	H., Wang, S., Huang, F., & Li, M. (2023). Satellite-Based Ranking of the World's
565	Hottest and Coldest Cities Reveals Inequitable Distribution of Temperature Extremes
566	Bulletin of the American Meteorological Society, 104(7), E1268–E1281.
567	https://doi.org/10.1175/bams-d-22-0233.1
568	Li, Y., Yang, T., Zhao, G., Ma, C., Yan, Y., Xu, Y., Wang, L., & Wang, L. (2024). A
569	systematic review of studies involving canopy layer urban heat island: Monitoring

570	and associated factors. Ecological Indicators, 158, 111424.
571	https://doi.org/10.1016/j.ecolind.2023.111424
572	Martilli, A., Krayenhoff, E. S., & Nazarian, N. (2020). Is the Urban Heat Island intensity
573	relevant for heat mitigation studies? Urban Climate, 31, 100541.
574	https://doi.org/10.1016/j.uclim.2019.100541
575	Masterton, J. M., & Richardson, F. (1981). Humidex: A method of quantifying human
576	discomfort due to excessive heat and humidity.
577	McGregor, G. R., & Vanos, J. K. (2018). Heat: A primer for public health researchers. <i>Public</i>
578	Health, 161, 138–146.
579	Meier, F., Fenner, D., Grassmann, T., Otto, M., & Scherer, D. (2017). Crowdsourcing air
580	temperature from citizen weather stations for urban climate research. Urban Climate,
581	19, 170–191. https://doi.org/10.1016/j.uclim.2017.01.006
582	Mohajerani, A., Bakaric, J., & Jeffrey-Bailey, T. (2017). The urban heat island effect, its
583	causes, and mitigation, with reference to the thermal properties of asphalt concrete.
584	Journal of Environmental Management, 197, 522–538.
585	https://doi.org/10.1016/j.jenvman.2017.03.095
586	Mukhopadhyay, B., & Weitz, C. A. (2022). Heat Exposure, Heat-Related Symptoms and
587	Coping Strategies among Elderly Residents of Urban Slums and Rural Vilages in
588	West Bengal, India. International Journal of Environmental Research and Public
589	Health, 19(19), 12446. https://doi.org/10.3390/ijerph191912446
590	Muller, C. L., Chapman, L., Grimmond, C. S. B., Young, D. T., & Cai, X. (2013). Sensors
591	and the city: A review of urban meteorological networks. International Journal of
592	Climatology, 33(7), 1585–1600. https://doi.org/10.1002/joc.3678

593	Muñoz Sabater, J. (2019). ERA5-Land hourly data from 1950 to present. Copernicus Climate
594	Change Service (C3S) Climate Data Store (CDS). [Dataset].
595	https://doi.org/10.24381/cds.e2161bac
596	Nan, F., Zeng, C., Shen, H., & Lin, L. (2025). Calibration of Integrated Low-Cost
597	Environmental Sensors for Urban Air Temperature Based on Machine Learning.
598	Sensors, 25(11), 3398. https://doi.org/10.3390/s25113398
599	Napoly, A., Grassmann, T., Meier, F., & Fenner, D. (2018). Development and Application of
600	a Statistically-Based Quality Control for Crowdsourced Air Temperature Data.
601	Frontiers in Earth Science, 6, 118. https://doi.org/10.3389/feart.2018.00118
602	Narayanan, A., Rezaali, M., Bunting, E. L., & Keellings, D. (2025). It's getting hot in here:
603	Spatial impact of humidity on heat wave severity in the U.S. Science of The Total
604	Environment, 963, 178397. https://doi.org/10.1016/j.scitotenv.2025.178397
605	Nielsen-Kellerman. (2020). Kestrel DROP wireless environmental data loggers: Certificate
606	of conformity and product specifications. Document No. 329004_9_2020.07.03.
607	https://kestrelinstruments.com
608	Nogueira, M., Hurduc, A., Ermida, S., Lima, D. C. A., Soares, P. M. M., Johannsen, F., &
609	Dutra, E. (2022). Assessment of the Paris urban heat island in ERA5 and offline
610	SURFEX-TEB (v8.1) simulations using the METEOSAT land surface temperature
611	product. Geoscientific Model Development, 15(14), 5949–5965.
612	https://doi.org/10.5194/gmd-15-5949-2022
613	Peel, M. C., Finlayson, B. L., & McMahon, T. A. (2007). Updated world map of the Köppen-
614	Geiger climate classification. Hydrology and Earth System Sciences, 11(5), 1633-
615	1644. https://doi.org/10.5194/hess-11-1633-2007

616	Romero Rodríguez, L., Sánchez Ramos, J., Sánchez De La Flor, F. J., & Álvarez Domínguez,
617	S. (2020). Analyzing the urban heat Island: Comprehensive methodology for data
618	gathering and optimal design of mobile transects. Sustainable Cities and Society, 55,
619	102027. https://doi.org/10.1016/j.scs.2020.102027
620	Rothfusz, L. P. (1990). The Heat Index "Equation" (or, More Than You Ever Wanted to
621	Know About Heat Index). National Oceanic and Atmospheric Administration,
622	National Weather Service, Office of Meteorology.
623	Segura, R., Krayenhoff, E. S., Martilli, A., Badia, A., Estruch, C., Ventura, S., & Villalba, G.
624	(2022). How do street trees affect urban temperatures and radiation exchange?
625	Observations and numerical evaluation in a highly compact city. Urban Climate, 46,
626	101288. https://doi.org/10.1016/j.uclim.2022.101288
627	Shandas, V., Voelkel, J., Williams, J., & Hoffman, J. (2019). Integrating Satellite and Ground
628	Measurements for Predicting Locations of Extreme Urban Heat. Climate, 7(1), 5.
629	https://doi.org/10.3390/cli7010005
630	Sherwood, S. C. (2018). How Important Is Humidity in Heat Stress? <i>Journal of Geophysical</i>
631	Research: Atmospheres, 123(21), 11,808-11,810.
632	https://doi.org/10.1029/2018JD028969
633	Shi, R., Hobbs, B. F., Zaitchik, B. F., Waugh, D. W., Scott, A. A., & Zhang, Y. (2021).
634	Monitoring intra-urban temperature with dense sensor networks: Fixed or mobile? An
635	empirical study in Baltimore, MD. Urban Climate, 39, 100979.
636	https://doi.org/10.1016/j.uclim.2021.100979
637	Steadman, R. G. (1979). The Assessment of Sultriness. Part I: A Temperature-Humidity
638	Index Based on Human Physiology and Clothing Science. Journal of Applied

639	Meteorology, 18(7), 861-873. https://doi.org/10.1175/1520-
640	0450(1979)018%253C0861:TAOSPI%253E2.0.CO;2
641	Stewart, I. D. (2011). A systematic review and scientific critique of methodology in modern
642	urban heat island literature. <i>International Journal of Climatology</i> , 31(2), 200–217.
643	https://doi.org/10.1002/joc.2141
644	Sun, X., Yan, S., Wang, B., Xia, L., Liu, Q., & Zhang, H. (2015). Air Temperature Error
645	Correction Based on Solar Radiation in an Economical Meteorological Wireless
646	Sensor Network. Sensors, 15(8), 18114–18139. https://doi.org/10.3390/s150818114
647	Venter, Z. S., Chakraborty, T., & Lee, X. (2021). Crowdsourced air temperatures contrast
648	satellite measures of the urban heat island and its mechanisms. Science Advances,
649	7(22), eabb9569. https://doi.org/10.1126/sciadv.abb9569
650	Wang, X., Hsu, A., & Chakraborty, T. (2023). Citizen and machine learning-aided high-
651	resolution mapping of urban heat exposure and stress. Environmental Research:
652	Infrastructure and Sustainability, 3(3), 035003. https://doi.org/10.1088/2634-
653	4505/acef57
654	World Meteorological Organisation. (2023). Guide to Meteorological Instruments and
655	Methods of Observation.
656	Yamamoto, K., Togami, T., Yamaguchi, N., & Ninomiya, S. (2017). Machine Learning-
657	Based Calibration of Low-Cost Air Temperature Sensors Using Environmental Data
658	Sensors, 17(6), 1290. https://doi.org/10.3390/s17061290
659	Young, D. T., Chapman, L., Muller, C. L., Cai, XM., & Grimmond, C. S. B. (2014). A
660	Low-Cost Wireless Temperature Sensor: Evaluation for Use in Environmental

661	Monitoring Applications. Journal of Atmospheric and Oceanic Technology, 31(4),
662	938–944. https://doi.org/10.1175/JTECH-D-13-00217.1
663	Yulizar, D., Soekirno, S., Ananda, N., Prabowo, M. A., Perdana, I. F. P., & Aofany, D.
664	(2023). Performance Analysis Comparison of DHT11, DHT22 and DS18B20 as
665	Temperature Measurement. Advances in Physics Research, 37–45.
666	https://doi.org/10.2991/978-94-6463-232-3_5
667	Zumwald, M., Knüsel, B., Bresch, D. N., & Knutti, R. (2021). Mapping urban temperature
668	using crowd-sensing data and machine learning. Urban Climate, 35, 100739.
669	https://doi.org/10.1016/j.uclim.2020.100739
670	